Modelling of local carbon deposition on rough test limiter exposed to the edge plasma of TEXTOR

Shuyu Dai[1,2], A. Kirschner[2], D. Matveev[2,3], D. Borodin[2], C. Björkas[2,4], Jizhong Sun[1], Dezhen Wang[1*]

[1] Key Laboratory of Materials Modification by Laser, Ion and Electron Beams (Ministry of Education), School of Physics and Optoelectronic Technology, Dalian University of Technology, Dalian 116024, China

[2] Institut für Energie- und Klimaforschung – Plasmaphysik, Forschungszentrum Jülich, Association EURATOM-FZJ, Trilateral Euregio Cluster, D-52425 Jülich, Germany.

[3] Department of Applied Physics, Ghent University, Plateaustraat 22, B-9000 Ghent, Belgium

[4] Association EURATOM-Tekes, Department of Physics, P.O.B 64, 00014 University of Helsinki, Finland

* Email:wangdez@dlut.edu.cn

Abstract: A Monte-Carlo code called SURO has been developed to study the influence of surface roughness on the impurity deposition characteristic in fusion experiments. SURO uses the test particle approach to describe the impact of background plasma and the deposition of impurity particles on a sinusoidal surface. The local impact angle and dynamic change of surface roughness as well as surface concentrations of different species due to erosion and deposition are taken into account. Coupled with 3D Monte-Carlo code ERO, SURO was used to study the impact of surface roughness on ^{13}C deposition in $^{13}CH_4$ injection experiments in TEXTOR. The simulations showed that the amount of net deposited ^{13}C species increases with surface roughness. Parameter studies with varying ^{12}C and ^{13}C fluxes were performed to gain insight into impurity deposition characteristic on the rough surface. Calculations of the exposure time needed for surface smoothing for TEXTOR and ITER were also carried out for different scenarios.

Keywords: Monte Carlo methods, edge plasma, surface roughness

PACS: 52.65.Pp, 52.40.Hf, 52.55.-s

1. Introduction

Plasma facing components (PFCs) exposed to a severe radiation environment in fusion devices suffer from intense power and particle fluxes [1-5]. The interaction between the edge plasma and PFCs determines the lifetime of PFCs, which is a crucial parameter for the viability of a fusion reactor. Moreover, the eroded impurities can be transported over long distances and be co-deposited together with fuel species. The resulting build-up of tritium-rich layers could become the main limiting factor for reactor availability due to safety restrictions. Therefore, studies of impurity transport, re-deposition and re-erosion are crucial to get a better understanding of underlying mechanisms

involved and to be able to adopt effective measures to minimize the tritium retention and net erosion.

Experimental observations indicated the influence of surface roughness on erosion and deposition. Results in TEXTOR [6], JET [7] and ASDEX Upgrade [8-9] revealed a strongly inhomogeneous erosion-deposition distribution with large erosion on protruding parts of the rough surface and deposition in recessions. Modelling has been performed to investigate this non-uniform erosion-deposition behaviour of impurities [10]. In addition, several simulation works have been carried out to study the development of the surface topography [11-13] and the impact of surface roughness on material sputtering [14-18].

Injection of tracer impurities such as $^{13}CH_4$ is a powerful tool to investigate impurity migration and deposition. The technique of ^{13}C injection through roof-like [19-20] and spherically shaped [21-22] test limiters in TEXTOR was applied to study the influence of various parameters such as substrate material, test limiter geometry, plasma conditions and also surface roughness on the local ^{13}C deposition. The local redeposition efficiency of ^{13}C showed that surface roughness increases the ^{13}C deposition efficiency on rough (~1μm) graphite surface by a factor of 3–5 compared with smooth (~0.1μm) one [22].

A Monte-Carlo code called SURO (abbreviated from SUrface ROughness), which takes into account the (re)erosion, (re)deposition and surface evolution of a rough surface, has been developed to study the effect of surface roughness on the ^{13}C deposition measured in TEXTOR experiments. The code can be combined with the three-dimensional (3D) Monte-Carlo code ERO [23], which simulates the transport of impurity particles in a given background plasma. The necessary input information for SURO (flux, angle and energy of impinging particles) is then provided by ERO. Modelling of the local deposition of ^{13}C has been carried out for various surface roughnesses and varying ^{12}C and ^{13}C fluxes. In addition, dynamic change of surface roughness has been studied.

2. The SURO code

The SURO code (2D in space and 3D in velocity) uses a sinusoidal surface of $z = a \sin(x/b)$ to describe the initial surface topography as shown in Fig.1 (a). The surface roughness (SR) is defined as the difference between the maximum and minimum points of the surface. Hence, the initial SR equals to 2a before the exposure. The initial directions of incoming particles are determined by the nominal angle α_{nom}, which is the angle between the incident direction and z-axis. The incident particles are launched from certain z location close to the surface and move along straight lines until they reach the surface. The effects of electromagnetic forces and resulting nominal angle distributions are treated in ERO code. When the incident particles reach the surface, the local angle α_{loc} is calculated according to the incident direction and the local surface normal at the impact position. The surface is divided into N bins in the x-direction (N is typically around 100). Every segment of the surface

has its own local surface normal vector, which is time dependent due to surface evolution under particle bombardment and resulting erosion/deposition. The time dependency is realized by dividing the SURO simulation into time steps Δt. As a result, the calculated local angles will be changed with dynamic evolution of each segment.

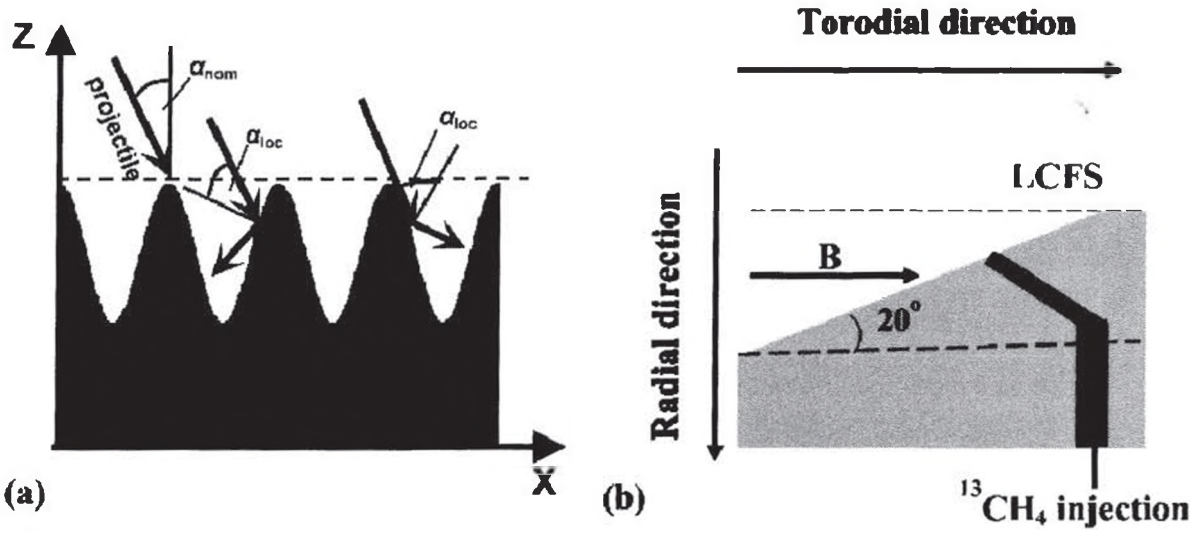

FIG. 1. The schematic of (a) surface topography of the substrate with a sinusoidal surface (b = 1.0 μm) and (b) experimental setup.

The physical sputtering yield due to impinging particles is based on the empirical formulae of Ref. [24]. The chemical erosion yield of graphite substrate by background deuterium ions bombardment is defined by an input parameter. For the simulations presented here, a chemical erosion yield of 1.5% is assumed, which is in general agreement with measured values in TEXTOR [25-26]. It is assumed that CD_4 molecules are generated in the process of chemical erosion [27-29]. A cosine angular distribution is assumed for the eroded particles. The Thompson and Maxwellian energy distributions are used for physically sputtered and chemically eroded particles, respectively [23]. Sticking or reflection of carbon atoms and hydrocarbons is determined by reflection coefficients taken from Ref. [30], which depend on species and incident energies and angles. It is assumed that the reflected particles obey the cosine angular distribution and the azimuthal direction continues in the forward direction of incident direction when reflected according to Refs. [31-32]. The particles are reflected with an energy typically around 32% of the incident energy based on Refs. [31-32].

For the modification of surface topography two correction procedures presented by T. Ishitani *et al* [7] have been taken into account in the model. First, it is necessary to remove the overmuch change of Δz which reverses the slope of the surface at each time step Δt. Second, an averaging technique is introduced for the calculation of Δz, so that $(\Delta z_{n-1} + 2\Delta z_n + \Delta z_{n+1})/4$ is

applied instead of Δz_n at the nth sampling point. These corrections are based on the practical situation that the sputtering process is determined by a collision cascade of finite dimensions. Therefore, the evolution of the apical point is affected by erosion/deposition of the neighboring segments.

The homogeneous mixing model (HMM) [29, 33-36] is used to consider mixing of different materials and to calculate their surface concentrations. For this, the substrate is divided into an interaction layer (the thickness of which is an input parameter) and a bulk volume. At the beginning of the exposure both the interaction layer and the bulk solely consist of substrate atoms. After the impact of impurities different species inside the interaction layer are distributed homogeneously. The total amount of particles in the interaction layer is kept constant, and accordingly, net erosion or deposition results in a shift of particles from the bulk into the interaction layer or from the interaction layer into the bulk, respectively. The concentrations of different species are updated after each time step. With increasing exposure time, the interaction layer reaches steady state and the concentrations of different species do not change anymore. The exposure time for reaching steady state is related to the interaction layer thickness since it is proportional to the total amount of particles in the interaction layer; however, the equilibrium concentrations of different species are independent of this thickness.

3. Simulation results

SURO is combined with ERO to study the deposition characteristic of ^{13}C particles on the smooth and rough test limiter surfaces resulting from $^{13}CH_4$ injection through these limiters. The simulation domain is divided into two regions: Scrape-Off Layer (SOL) plasma region, in which the transport of particles is treated by ERO, and a near surface region where the particles interact with the smooth or rough surfaces addressed by SURO. The current ERO version also can simulate the transport of background plasma particles by means of the test particle approach in order to calculate angular distribution when hitting the (smooth) surface. After reaching the surface, information about flux, angle and energy of deuterium and ^{12}C ions is stored and employed as input for SURO. Also, the transport of injected methane through the edge plasma is simulated by ERO. Part of injected species returns to the surface and again the information (species, angle, energy, charge) of returning ^{13}C species is used as input for SURO. The returning ^{13}C species include hydrocarbon ions and neutrals, and ionized and atomic carbon particles.

The simulation parameters used here for modelling the transport of impurities in ERO are on the basis of tracer injection experiments in TEXTOR [19-20], which had been performed to study the local transport and deposition behaviour of impurities. A defined number of $^{13}CH_4$ molecules is injected through a hole in a roof-like limiter plate with an inclination angle of 20° with respect to the magnetic field as shown in Fig.1 (b).

The magnetic field lies in x-z plane of Fig.1 (a). The tip of the test limiter is positioned at the last closed flux surface (LCFS) with a radial position of 0.46 m. The electron temperature (T_e = 54 eV), ion temperature (T_i = $1.5T_e$) and electron density (n_e = 1.9 × 10^{12} cm^{-3}) at the LCFS are used as input in the ERO modeling – these parameters represent typical ohmic discharge conditions. The exponential decay lengths are $\lambda_{T_{e,i}}$ = 40 mm and λ_{n_e} = 22 mm, respectively. The calculated debye length λ_D is around 40 μm and is much larger than surface roughness (~1 μm). In this case, it is assumed that the surface roughness does not significantly affect the E field [10]. The flux densities of background deuterium (carbon) ions are in the range from 8.6 × 10^9 $\mu m^{-2}s^{-1}$ (3.1 × 10^8 $\mu m^{-2}s^{-1}$) to 6.9 × 10^9 $\mu m^{-2}s^{-1}$ (1.8 × 10^8 $\mu m^{-2}s^{-1}$) in the simulations. The ^{12}C concentration at the LCFS is assumed to be 3.5% as reference case according to Refs. [37-38].

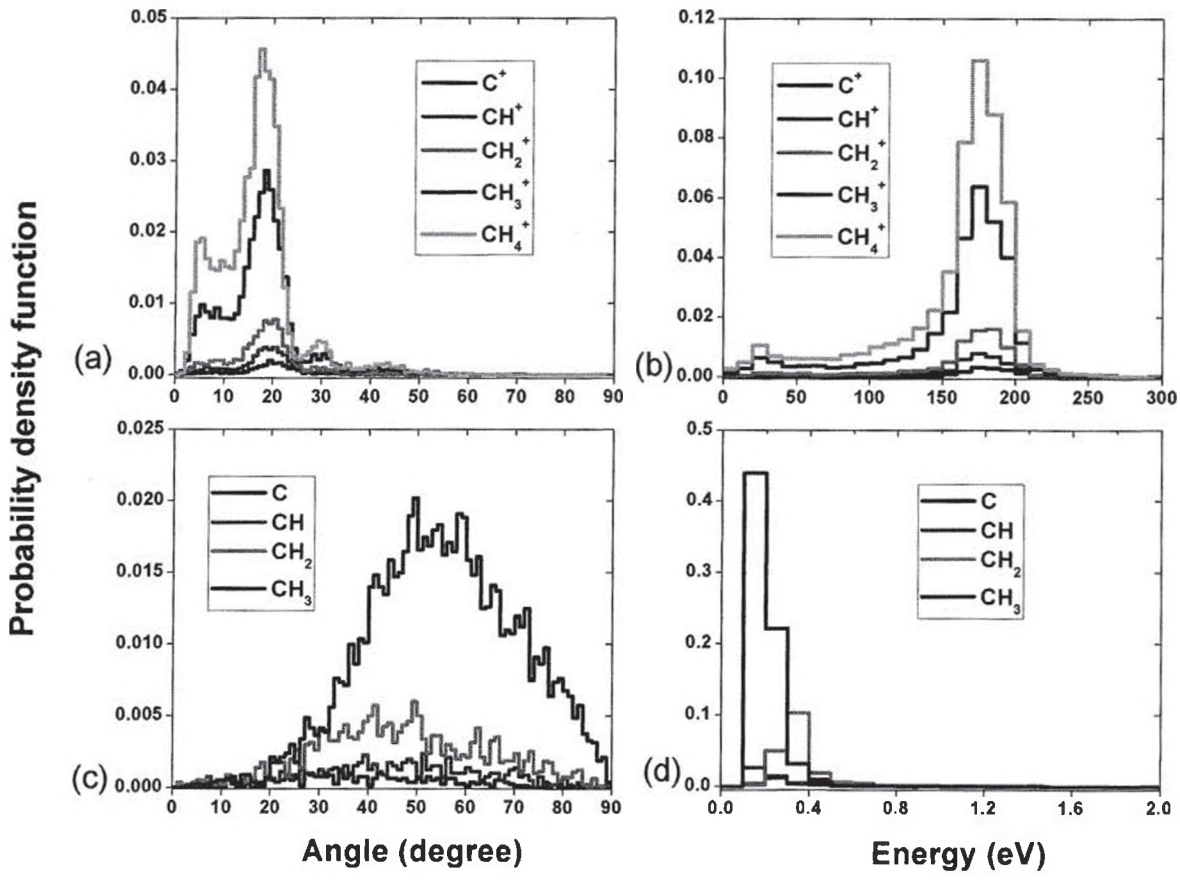

FIG. 2. The nominal angle and impact energy distributions of (a) (b) ionized ^{13}C species and (c) (d) neutral ^{13}C species returning to the surface.

3.1 ERO modelling: calculation of nominal angle and impact energy of returning ^{13}C species from $^{13}CH_4$ injection in TEXTOR

The spatial resolution of the limiter surface in ERO is determined by a surface net which divides the surface into predefined cells according to the input parameters.

Since the modelling dimension of ERO (~100 mm, surface cell size at limiter 3×3 mm^2) is much larger than that of SURO (~1μm), it is necessary to check whether different locations of predefined surface cells in ERO have significant difference in the nominal angle and impact energy distributions of returning ^{13}C species. However, the results from ERO reveal similar distributions for all the predefined surface cells as shown exemplarily in Fig.2, presenting the nominal angle and impact energy distributions of ionized and neutral ^{13}C species returning to the surface. Therefore, the location dependence of nominal angle and impact energy distributions of returning ^{13}C species can be neglected and the above results can be used as input data for SURO. As shown in Fig.2 (a) and (c), the ionized ^{13}C species have a much narrower nominal angle distribution compared to the neutral ones. The nominal angles for the ionized ^{13}C species are around 20° whereas the neutral ^{13}C species have a relatively uniform nominal angle distribution. In addition, the energies of the neutral ^{13}C species are mainly below 0.5 eV. The ionized ^{13}C species, which have been accelerated in the sheath potential, carry the kinetic energies in the range from 150 to 200 eV.

Figure3 (a) shows nominal angle distributions of background deuterium and background ^{12}C ions impinging on the smooth surface. The background deuterium and ^{12}C ions with a Maxwellian energy distribution are injected into the SOL far from the limiter surface (typical around 200 mm) and tracked until they reach the limiter surface. It is assumed that the charge state of ^{12}C ions is 3 in the simulation. It can be seen that the ^{12}C ions, whose maximum of angular distribution is located around 40°, have a relatively symmetric angular distribution. For deuterium ions, the maximum is located around 50°. The energies of deuterium and carbon ions impacting the surface are the sum of the thermal energy and energy gained by acceleration in the presheath and sheath: $E = 2T_i + \frac{1}{2}MV_s^2 + 3QT_e$, where M is the charge mass, V_s is the sound speed and Q is the charge state of the ion [39-40].

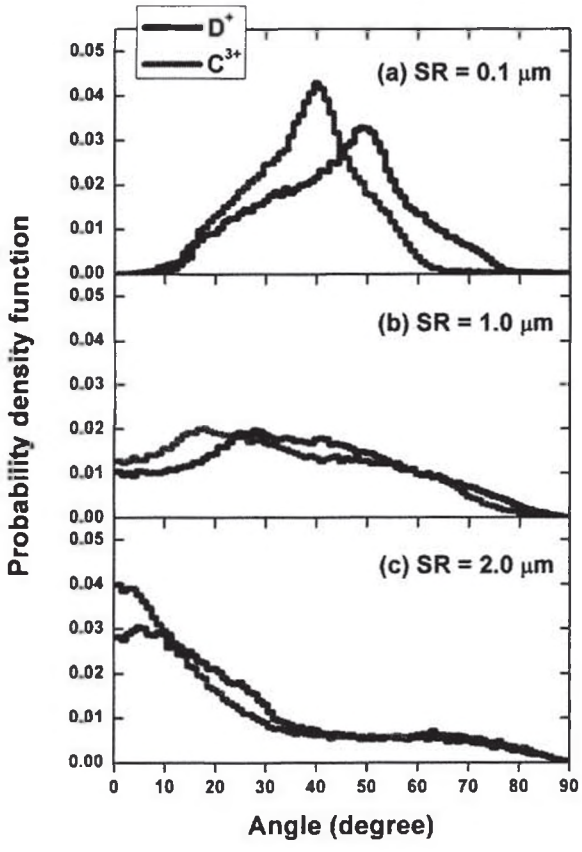

FIG. 3. The angular distributions of background D^+ and C^{3+} particles impinging on the (a) smooth (SR = 0.1 μm) and (b) (c) rough (SR = 1.0 μm, 2.0 μm) surfaces.

3.2 SURO modelling

3.2.1 Calculation of local impact angle

The angular distributions from ERO are used as nominal angles for SURO. The resulting local angle distributions for the background species obtained by SURO for SR = 1.0 and 2.0 μm are indicated in Fig.3 (b) and (c), respectively. It is seen that the local angle distributions of deuterium and ^{12}C ions demonstrate a strong dependence on the surface topography. With increasing SR, the peak values of angular distributions shift to smaller angles gradually. The peak values for SR = 1.0 μm are reduced compared to the smooth surface, and accordingly, the angular distribution becomes more uniform. The azimuthal direction of charged particles is along the forward direction of inclined B-field line (in x-z plane), and the azimuthal direction of neutral ones not constrained by B-field line is uniform. The gross physical sputtering yield (not considering redeposition) is related to the local impact angle according to Ref. [24]. The gross physical sputtering yields calculated with SURO integrated over all segments of the surface are, however, reduced marginally with increasing SR. All the values for smooth and rough surfaces are around 3% and 24% for D^+ and C^{3+}, respectively. Therefore, the influence of gross physical sputtering can be excluded here when comparing net deposited amount of ^{13}C species on the smooth and rough surfaces in the following analysis.

3.2.2 The influence of ^{13}C flux ratio

The effect the ^{13}C flux ratio has been investigated on the deposition of ^{13}C species on the smooth and rough surfaces. The ^{13}C flux ratio is defined as the ratio of ^{13}C flux returning to the surface to the background D^+ flux. Unless otherwise states, the simulations were performed for a total time of 500 s, which is long enough to reach steady state in the interaction layer such that the surface concentrations of different species do not change anymore. As shown in Fig.4, the amount of net deposited ^{13}C species on the rough surface is larger than that on the smooth one. The mechanism of enhanced re-deposition on the rough surface [12-13, 22] is the reason why the amount of net deposited ^{13}C species becomes greater. All reflected and re-eroded ^{13}C species from a smooth surface can "escape" easily while for a rough surface a certain amount will scrape the local wrinkles and thus be re-deposited. Larger SR reduces the probability for ^{13}C species to directly escape from the valley. In addition, it will intensify the trapping ability of rough surface because ^{13}C species experience more reflections through a ping-pong transport between the ridges of rough surface.

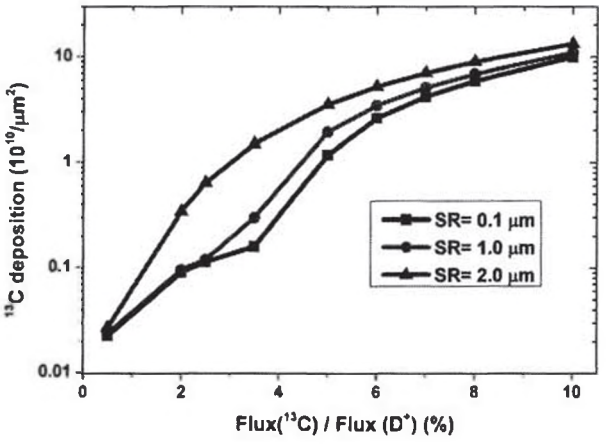

FIG. 4. The ^{13}C deposition as a function of ^{13}C flux ratio for the smooth and rough surfaces. The

concentration of background ^{12}C ions at the LCFS is 3.5%.

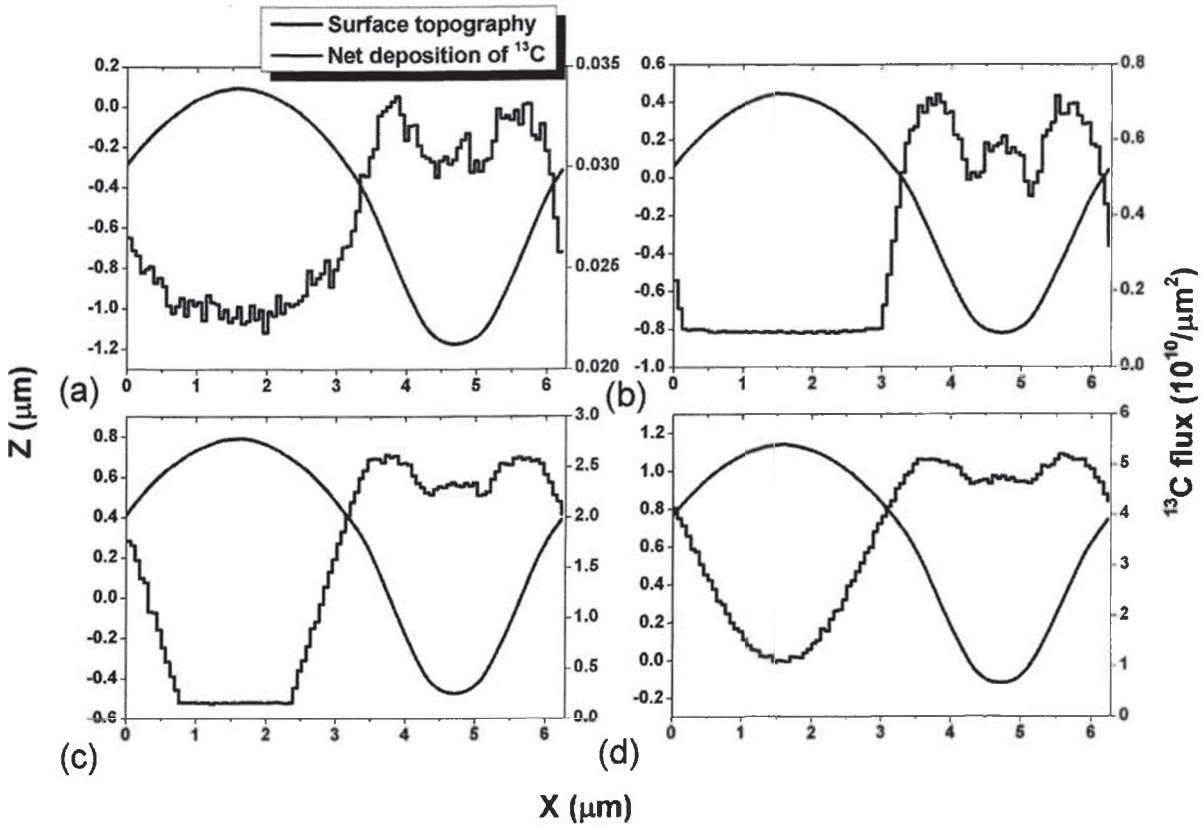

FIG. 5. Profiles of surface topography and net deposited ^{13}C areal density after 500 s exposure for initial SR = 2.0 μm with ^{13}C flux ratios (a) 0.5%, (b) 2.0%, (c) 3.5% and (d) 5.0%. The concentration of background ^{12}C ions at the LCFS is 3.5%.

Figure 5 presents the surface topography and net deposited ^{13}C areal density after 500 s exposure for initial SR = 2.0 μm with different ^{13}C flux ratios. It is obvious that the net deposited ^{13}C fluxes are larger at surface recessions, which is in support of the above-mentioned mechanism of enhanced re-deposition of ^{13}C species on the rough surface. The symmetrical profile of net deposited ^{13}C areal density in Fig.5 is due to the correlation between incident direction (i.e. nominal angle) and topography of rough surface. Since the valley of rough surface is open compared with the nominal angles which are calculated by ERO in Fig.2 and 3, the incident particles can reach both ridges of rough surface as shown schematically in Fig.1 (a). As a result, the symmetrical profile is obtained as shown in Fig.5.

Figure 6 shows the normalized ^{13}C deposition as a function of ^{13}C flux ratios for initial SR = 2.0 μm with different ^{12}C concentrations at the LCFS. The normalized ^{13}C deposition, which is used for a direct comparison of the difference in ^{13}C deposition characteristic between the smooth and rough surfaces, is defined as the ratio of the amount of net deposited ^{13}C species on the rough surface to that on the smooth

one. The normalized ^{13}C deposition first increases and then decreases with ^{13}C flux ratio for all assumptions of ^{12}C concentration. Furthermore, we find that the flux ratios of $(^{13}C+^{12}C)/D^{+}$ at SURO surface, which are calculated by SURO, are kept around 8% for all the maxima of the normalized ^{13}C deposition. This finding indicates that the difference in the amount of net deposited ^{13}C species on the smooth and rough surfaces is dependent on the ratio of $(^{13}C+^{12}C)/D^{+}$.

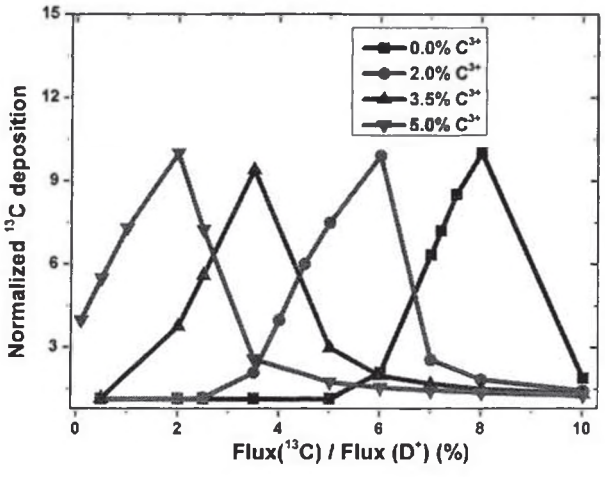

FIG. 6. The normalized ^{13}C deposition as a function of ^{13}C flux ratio for initial SR = 2.0 μm. The concentrations of background ^{12}C ions at the LCFS are 0%, 2.0%, 3.5% and 5.0%.

This phenomenon can be explained with the help of Fig.7 which illustrates the time-evolution of the surface topography for initial SR = 2.0 μm with different ^{13}C flux ratios. At the beginning, there are net deposited ^{13}C species in the surface due to a small ^{13}C surface concentration and with increasing exposure time, the surface concentration of ^{13}C species increases because of subsequent injection, which, in turn, leads to erosion of an increased number of ^{13}C species. After a certain time, the amount of net deposited ^{13}C species does not change anymore and steady state is reached. For a case of small ^{13}C flux ratio in Fig.7 (a), the calculations reveal that both the hills and recessions of rough surface suffer from net erosion. Hence, the amount of net deposited ^{13}C species on the rough surface is similar to that on the smooth surface, which results in small normalized ^{13}C deposition as shown in Fig.6. As the ^{13}C flux ratios increase as shown in Fig.7 (b) and (c), the hills of the rough surface still undergo net erosion while the valley regions are subject to net deposition. The smooth surface still suffers from net erosion (the erosion-dominated case) when the ^{13}C flux ratio is below 8% (data not shown). Therefore, the amount of the deposited ^{13}C species is much larger for the rough surface which leads to a higher normalized ^{13}C deposition. While for an even higher ^{13}C flux ratio of 8%, both the hill and valley regions receive net deposition; meanwhile, the smooth surface also receives net deposition (the deposition-dominated case). As a result, the normalized ^{13}C deposition is reduced correspondingly as shown in Fig.6.

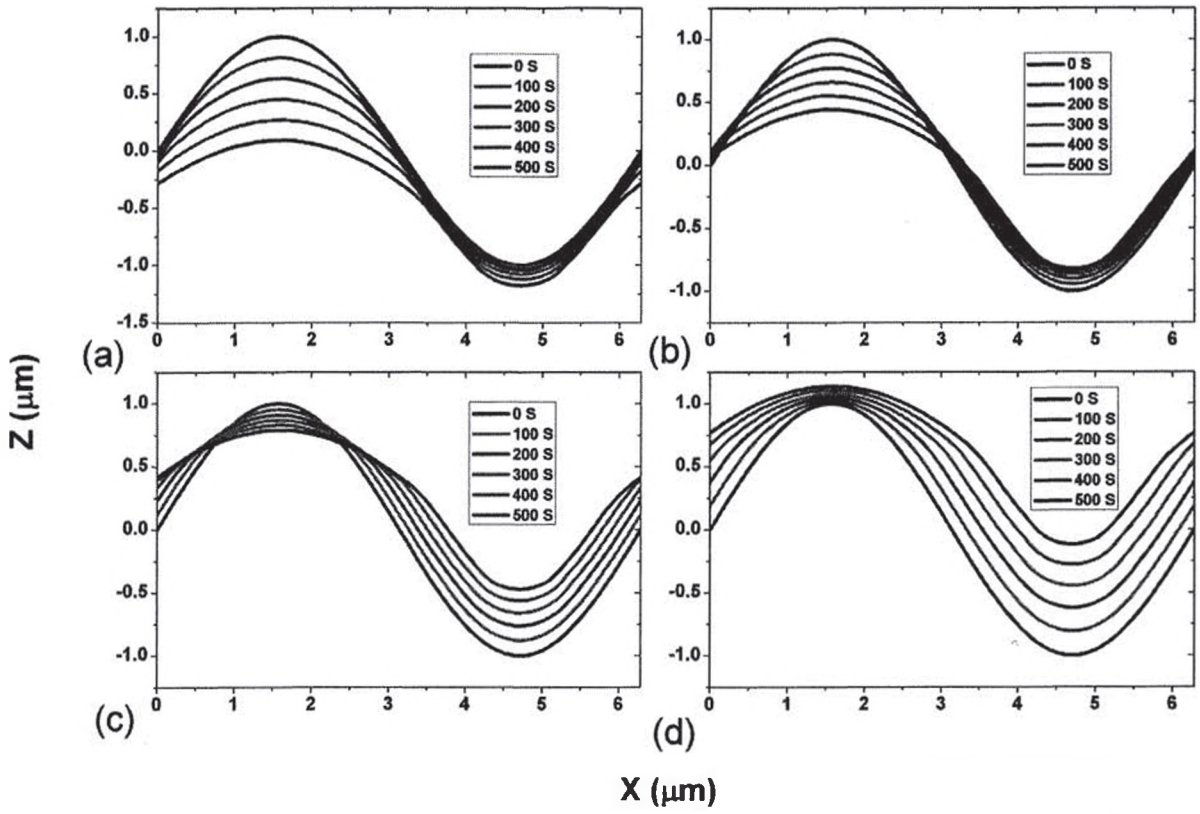

FIG. 7. Profiles of the time-evolution of surface topography for initial SR = 2.0 μm with ^{13}C flux ratios (a) 0.5%, (b) 2.0%, (c) 3.5% and (d) 5.0%. The concentration of background ^{12}C ions at the LCFS is 3.5%.

3.2.3 The influence of background ^{12}C concentration

The ^{12}C concentration in the background plasma is an important input parameter for the modelling. We therefore made a parameter study by varying this concentration and observing the effect on the deposition of ^{13}C species on the smooth and rough surfaces. Three background ^{12}C concentrations of 2.0%, 3.5% and 5.0% at the LCFS were used and these concentrations were assumed to increase exponentially with a decay length of ~14cm when going further into the SOL [41]. SURO was applied to an ERO surface cell located at a distance of 18 mm from the LCFS in the radial direction and the corresponding background ^{12}C concentrations at the SURO surface are 2.3%, 4.0% and 5.7%, respectively. Figure 8 illustrates the ^{13}C deposition as a function of ^{12}C concentration at the LCFS for the smooth and rough surfaces. It can be seen that the ^{13}C deposition increases with background ^{12}C concentration. This can be explained by the fact that a larger background ^{12}C concentration results in a higher ^{12}C concentration in the surface. Correspondingly, the resulting reduction of the ^{13}C surface concentration leads to a reduced erosion of ^{13}C species and thus a greater amount of net deposited ^{13}C species. In addition, the above interpretation also can be used to make clear the reason why a larger background ^{12}C concentration along with a reduced ^{13}C flux ratio leads to the maximum of the normalized ^{13}C

deposition in Fig.6.

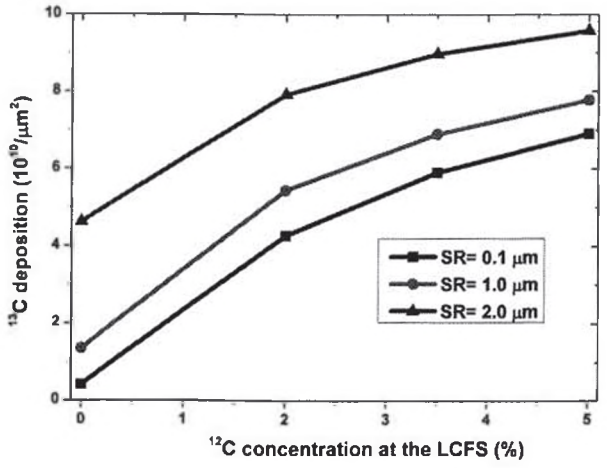

FIG. 8. The ^{13}C deposition as a function of ^{12}C concentration at the LCFS for the smooth and rough surfaces. The ^{13}C flux ratio of 8% is used.

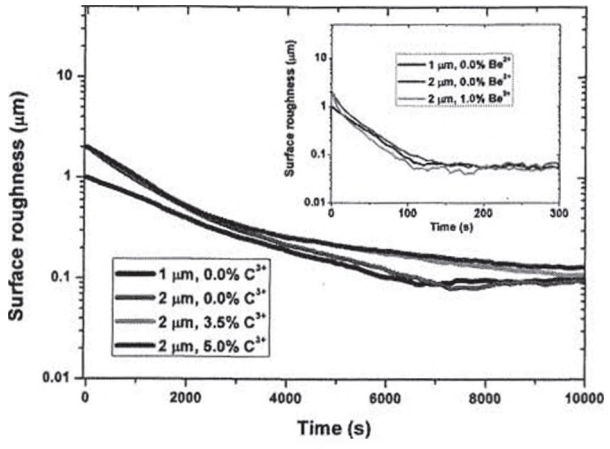

FIG. 9. The profile of the time-evolution of SR for initial SR = 1.0 and 2.0 μm with different ^{12}C concentrations at the LCFS (0%, 3.5% and 5.0%) for TEXTOR case. The inset graph shows the time-evolution of SR for initial SR = 1.0 and 2.0 μm with different Be^{2+} concentrations (0% and 1.0%) in the edge plasma for ITER inner divertor case.

3.2.4 Calculation of the exposure time for surface smoothing for TEXTOR and ITER

The erosion-deposition distribution is inhomogeneous due to surface roughness as shown in Fig.7, with a high erosion or small deposition on protruding parts of rough surface, and a lower erosion or larger deposition at the far side of ridges and at the bottom of recessions. A similar phenomenon is also observed in different tokamak facilities [6-9], which may finally lead to a smoothing of initially rough surface. This effect of long pulse and steady state operation is difficult to study in present tokamak facilities, but predictive modelling can be performed to investigate it.

The time-evolution of SR for initial SR = 1.0 and 2.0 μm with different ^{12}C concentrations at the LCFS in TEXTOR is presented in Fig.9. There are no injected ^{13}C particles for assessing surface smoothing during routine operation of fusion devices. The interaction layer thickness is assumed to be 40 nm in the HMM. Since the exposure time for reaching steady state of surface concentrations is much shorter than that for the smoothing of rough surface, the interaction layer thickness does not have a strong impact on the exposure time for surface smoothing. It is clearly shown that the SR first reduces very sharply before 2000 s, and then its reduction speed becomes slow between 2000-7000 s. Eventually, the steady state of surface topography is reached where the SR does not change anymore. In addition, the inset graph of Fig.9 shows the time-evolution of SR for initial SR = 1.0 and 2.0 μm with different Be^{2+} concentrations in the edge plasma for ITER inner divertor. This modelling was performed using typical plasma edge parameters in ITER based on the Refs. [29, 34]. The modelling location

is chosen to be at the strike point area that receives the maximum particle flux. The Be^{2+} concentration is the ratio of influx of Be^{2+} into the divertor to the deuterium ion flux. As shown in the inset graph, there is also a continuous reduction of the SR with exposure time until an equilibrium value is reached. The exposure time of about 100 s for reaching steady state decreases greatly compared with the TEXTOR case since the particle flux increases by two orders of magnitude.

4. Summary and discussion

The Monte-Carlo code SURO was developed and combined with ERO to investigate the influence of surface roughness on the ^{13}C deposition characteristic in $^{13}CH_4$ injection experiments in TEXTOR. Comprehensive parameter variations, such as different surface roughnesses, ^{13}C flux ratios and background ^{12}C concentrations, were performed to study their effects on the deposition of ^{13}C species. It was seen that the variation of local angle of background deuterium and ^{12}C ions due to surface topography does not have a strong impact on the gross physical sputtering yield, which can therefore be excluded in the analysis of the difference in ^{13}C deposition characteristic between smooth and rough surfaces. The results also showed that the amount of net deposited ^{13}C species increases with surface roughness and that there are more net deposited ^{13}C species at surface recessions due to enhanced re-deposition on rough surfaces. A larger surface roughness can intensify the trapping ability of ^{13}C species which experience more reflections caused by a ping-pong transport between the ridges of rough surface. The variation of the ratio of $(^{13}C+^{12}C)/D^+$ leads to a corresponding change in the normalized ^{13}C deposition (the deposition on the rough surface compared to the smooth one). With increasing $(^{13}C+^{12}C)/D^+$, the rough surface experiences an erosion-dominated case, intermediate state (half erosion and half deposition case) and deposition-dominated case, which is determined by the balance of incoming and outgoing particle fluxes. Furthermore, the amount of net deposited ^{13}C species showed a clear dependence on background ^{12}C concentration, which plays a protective role in the erosion of deposited ^{13}C species. An increased background ^{12}C concentration results in a reduced ^{13}C flux ratio for the maximum of the normalized ^{13}C deposition. For TEXTOR conditions, the exposure time for smoothening of the rough surface was around 7000 s, which is two orders of magnitude larger than that for an ITER case.

Experimental results in TEXTOR have shown that surface roughness leads to increased ^{13}C deposition efficiency [22]. The surface roughness is on the micron scale, which makes it difficult to reproduce the experimental result in a much larger scale. However, the experimental result can be explained qualitatively on the basis of the current modelling. Since the area around the injection hole is in the deposition-dominated case due to great ^{13}C incident flux, almost the same deposited ^{13}C amounts are obtained in the same area for the smooth and rough

surfaces according to the above modelling results (Fig.6). This is also supported by the experimental result which showed that the difference in the ^{13}C deposition efficiency is mainly due to a wider deposition pattern on the rough surface compared with the smooth one, which indicates that the deposited ^{13}C amounts in the same area around the injection hole are similar for the smooth and rough surfaces. The areal expansion of ^{13}C deposition is caused by a step-wise transport through a repetitive process of erosion of ^{13}C species from the layer and its subsequent re-deposition nearby. During this step-wise transport, the gradual reduction of ^{13}C incident flux leads to the rough surface far from the injection hole turning into the intermediate state, whereas the smooth surface is in the erosion-dominated case. Therefore, some deposited ^{13}C species on the rough surface can survive re-erosion of background plasma due to the trapping effect of rough surface. The wider deposition pattern of ^{13}C deposition on the rough surface supports this interpretation experimentally.

Acknowledgements

This work was supported by National Magnetic Confinement Fusion Science Program No. 2013GB109001, National Natural Science Foundation of China under Grant No.11275042 and Chinese Scholarship Council. This work was partly supported by the JSPS-NRF-NSFC A3 Foresight Program in the field of Plasma Physics (NSFC: No.11261140328). Authors would like to express their appreciation to F. Wang, Z.F. Yao and A. Kreter for their assistance in computation and helpful discussions.

Reference

[1] Federici G, Skinner C H, Brooks J N *et al* 2001 *Nucl.Fusion* **41** 1967

[2] Shimada M, Campbell D J, Mukhovatov V *et al* 2007 *Nucl.Fusion* **47** S1

[3] Roth J, Tsitrone E, Loarer T *et al* 2008 *Plasma Phys. Control. Fusion* **50** 103001

[4] Roth J, Tsitrone E, Loarte A *et al* 2009 *J. Nucl. Mater.* **390-391** 1

[5] Merola M, Loesser D, Martin A *et al* 2010 *Fusion Eng. Des.* **85** 2312-2322

[6] Wienhold P, Weschenfelder F, Karduck P *et al* 1999 *J. Nucl. Mater.* **266–269** 986

[7] Mayer M, Likonen J, Coad J P *et al* 2007 *J. Nucl. Mater.* **363–365** 101

[8] Mayer M, Rohde V, Ramos G *et al* 2007 *Phys. Scr.* **T 128** 106

[9] Mayer M, Andrzejczuk M, Dux R *et al* 2009 *Phys. Scr.* **T 138** 014039

[10] Schmid K, Mayer M, Adelhelm C *et al* 2010 *Nucl.Fusion* **50** 105004

[11] Nobes M J, Colligon J S, Carter G 1969 *J. Mater.Sci.* **4** 730-733

[12] Ishitani T, Kato M, Shimizu R 1974 *J. Mater.Sci.* **9** 505

[13] Ohya K, Kawakami R, Aizawa H, 2000 *J. Plasma Fusion Res. SERIES* **3** 288

[14] Ruzic D N and Chiu H K 1989 *J. Nucl. Mater.*

162-164 904

[15] Brooks J N and Ruzic D N 1990 *J. Nucl. Mater.* **176-177** 278

[16] Ruzic D N 1990 *Nucl. Instrum. Methods B* **47** 118

[17] Küstner M, Eckstein W, Dose V and Roth J 1998 *Nucl. Instrum. Methods B* **145** 320

[18] Küstner M, Eckstein W, Hechtl E and Roth J 1999 *J. Nucl. Mater.* **265** 22

[19] Wienhold P, Esser H G, Hildebrandt D *et al* 2001 *J. Nucl. Mater.* **290-293** 362

[20] Kreter A, Wienhold P, Borodin D *et al* 2007 *J. Nucl. Mater.* **363–365** 179

[21] Kreter A, Borodin D, Brezinsek S *et al* 2006 *Plasma Phys. Control. Fusion* **48** 1401

[22] Kreter A, Brezinsek S, Hirai T *et al* 2008 *Plasma Phys. Control. Fusion* **50** 095008

[23] Kirschner A, Philipps V, Winter J *et al* 2000 *Nucl.Fusion* **40** 989

[24] García-Rosales C, Eckstein W and Roth J 1994 *J. Nucl. Mater.* **218** 8-17

[25] Pospieszczyk A, Philipps V, Casarotto E *et al* 1997 *J. Nucl. Mater.* **241–243** 833

[26] Brezinsek S, Posieszczyk A, Borodin D *et al* 2007 *J. Nucl. Mater.* **363–365** 1119

[27] Ohya K, Inai K, Inoue M *et al* 2011 *J. Nucl. Mater.* **417** 602

[28] Inai K, Ohya K, Tomita Y *et al* 2009 *J. Nucl. Mater.* **390-391** 119

[29] Kirschner A, Borodin D, Droste S *et al* 2007 *J. Nucl. Mater.* **363–365** 91

[30] Ohya K, Kikuhara Y, Inai K *et al* 2009 *J. Nucl. Mater.* **390–391** 72

[31] Alman D A, Ruzic D N, 2003 *J. Nucl. Mater.* **313-316** 182

[32] Alman D A, Ruzic D N, 2004 *Phys. Scr.* **T111** 145

[33] Droste S, Borodin D, Kirschner A *et al* 2006 *Contrib. Plasma Phys.* **46** 628

[34] Kirschner A, Borodin D, Philipps V *et al* 2009 *J. Nucl. Mater.* **390–391** 152

[35] Kirschner A, Ohya K, Borodin D *et al* 2009 *Phys. Scr.* **T138** 014011

[36] Matveev D, Kirschner A, Litnovsky A *et al* 2010 *Plasma Phys. Control. Fusion* **52** 075007

[37] Ding R *et al* 2010 *Plasma Phys. Control. Fusion* **52** 045005

[38] Droste S *et al* 2008 *Plasma Phys. Control. Fusion* **50** 015006

[39] Stangeby P C, 2000 *The Plasma Boundary of Magnetic Fusion Devices* (Bristol: Institute of physics Publishing)

[40] Warrier M, Schneider R, Bonnin X, 2004 *COMPUT. PHYS. COMMUN* **160** 46

[41] Wienhold P 1989 *J. Nucl. Mater.* **162-164** 369